Scaling Up Soft Robotics

A Meter-Scale, Modular, and Reconfigurable Soft Robotic System

Li, Shuguang; Awale, Samer A.; Bacher, Katharine E.; Buchner, Thomas J.; Della Santina, Cosimo; Wood, Robert J.; Rus, Daniela

DOI
10.1089/soro.2020.0123

Publication date
2022

Document Version
Final published version

Published in
Soft Robotics

Citation (APA)
Li, S., Awale, S. A., Bacher, K. E., Buchner, T. J., Della Santina, C., Wood, R. J., & Rus, D. (2022). Scaling Up Soft Robotics: A Meter-Scale, Modular, and Reconfigurable Soft Robotic System. *Soft Robotics*, *9*(2), 324-336. https://doi.org/10.1089/soro.2020.0123

SOFT ROBOTICS
Volume 00, Number 00, 2021

DOI: 10.1089/soro.2020.0123

SoRo
Soft Robotics

Scaling Up Soft Robotics: A Meter-Scale, Modular, and Reconfigurable Soft Robotic System

Shuguang Li,[1,2] Samer A. Awale,[2,*] Katharine E. Bacher,[2,*] Thomas J. Buchner,[2,3,*] Cosimo Della Santina,[2,4,5] Robert J. Wood,[1] and Daniela Rus[2]

Abstract

Today's use of large-scale industrial robots is enabling extraordinary achievement on the assembly line, but these robots remain isolated from the humans on the factory floor because they are very powerful, and thus dangerous to be around. In contrast, the soft robotics research community has proposed soft robots that are safe for human environments. The current state of the art enables the creation of small-scale soft robotic devices. In this article we address the gap between small-scale soft robots and the need for human-sized safe robots by introducing a new soft robotic module and multiple human-scale robot configurations based on this module. We tackle large-scale soft robots by presenting a modular and reconfigurable soft robotic platform that can be used to build fully functional and untethered meter-scale soft robots. These findings indicate that a new wave of human-scale soft robots can be an alternative to classic rigid-bodied robots in tasks and environments where humans and machines can work side by side with capabilities that include, but are not limited to, autonomous legged locomotion and grasping.

Keywords: soft robotics, legged locomotion, soft grasping, soft actuators, modular robotics

Introduction

Soft robotics is a nascent subfield of robotics focusing on robots made primarily out of soft, flexible, and deformable materials.[1–4] Typical materials used in this field[5,6]—foam, rubber, and fabric—can be dropped, squashed, bent, squeezed, and deformed in many other ways without losing their original shape. Breaking away from the traditional paradigm of rigid-bodied robots, and with the potential of achieving new levels of flexibility, adaptability, and safety, soft robotics promises to be a game-changing technology.

Developing soft robots able to operate at human scales represents a fundamental step toward providing a credible alternative to traditional rigid-bodied robots. The current state of soft robotics, however, faces significant challenges with scale and size. Much research exists on the design of soft robots with bodies ranging from millimeter[7,8] to submeter size.[9] The use of light-weight flexible materials and the development of untethered powerful soft actuators are two promising approaches to address this challenge.

Most recent research relies on silicone rubber-based pneumatic actuators, which get very heavy when scaled up (silicone rubber's density >1000 kg/m^3). Large systems made from these actuators would have trouble lifting their own weight. Thus, many soft robots using these types of actuators tend to be at most several centimeters.[10–12] Scaling to large dimensions is also a well-known limitation of soft actuators made of electroactive polymers,[13] which are typically used to build soft robots at millimeter or centimeter scales.[14]

Recently, balloon-like inflatable structures are being investigated as a means to achieve large-scale light-weight soft

[1]John A. Paulson School of Engineering and Applied Sciences, and the Wyss Institute for Biologically Inspired Engineering, Harvard University, Cambridge, Massachusetts, USA.
[2]Computer Science and Artificial Intelligence Laboratory, Massachusetts Institute of Technology, Cambridge, Massachusetts, USA.
[3]Department of Physics and Munich School of BioEngineering, Technical University of Munich, Garching, Germany.
[4]Institute of Robotics and Mechatronics, German Aerospace Center, Oberpfaffenhofen, Germany.
[5]Cognitive Robotics Department, Delft University of Technology, Delft, The Netherlands.
*These authors contributed equally to this study.

robots. Examples of such balloon-bodied soft robots include the vine robot,[15] the isoperimetric robot,[16] the Giacometti arm,[17] the inflatable manipulator developed at Carnegie Mellon University,[18] the Ant-Roach walking robot,[19] and the inflatable humanoid robot—King Louie.[20,21] The isoperimetric robot is capable of shape change by continuously relocating its joints (rigid roller modules) along the inflatable tubes, therefore, it can operate without compressing air or requiring a tether. However, most of these large soft robots are only able to carry very light payloads (e.g., small cameras). With additional high-pressure pneumatic actuators, a few of them can carry or manipulate heavier objects.[19–21] Nevertheless, all of these powerful actuators need to be driven and controlled by tethered external pneumatic sources and components, including pumps, compressors, regulators, and valves. The tether constraints and insufficient strengths inevitably limit the applications of these large soft robots.

Building such a large, untethered, and versatile soft-bodied robot is a challenge,[9,22] which nature itself rarely tackles. Large-scale soft-bodied animal parts—namely muscular and skeletal hydrostats[23]—are very rare outside of water. A notable example is the trunk of elephant, which is carried by a vertebrate body. Artificial systems, however, can leverage a vast array of innovative materials and actuation strategies, to possibly enable solutions imitating or even surpassing those of animals. In this study, we push the boundaries of soft robotics to the meter scale by proposing a general-purpose solution for building untethered, modular, reconfigurable, and—most importantly—large soft robotic platforms (Fig. 1). Modularity is a key ingredient in this framework since it allows for the fast and intuitive realization of a complex robot by simple interconnection of self-contained components.[24,25] Leveraging the advantages of both soft and modular robotics will provide our system a high level of adaptivity and flexibility that is not traditionally found in rigid robots.[26–36] With this in mind, we design a large-scale vacuum-driven soft robotic module (dimension: $0.15\,\text{m} \times 0.15\,\text{m} \times 0.86\,\text{m}$, weight: 1.6 kg), which can bend in eight directions (maximum bending angle $\approx 30°$), contract longitudinally (maximum contraction ratio $\approx 7\%$), and connect to other modules. We then build a group of such soft modules, and each module is equipped with actuation, proprioceptive sensing, intermodule communication, and computation, allowing for autonomous configuration control. We demonstrate that these soft modules can be rapidly aggregated into a variety of self-contained meter-scale soft robots on demand, such as a hexapod robot, a large gripper, and a crawling robot. Moreover, we develop planning and control algorithms that enable these meter-scale soft robots to autonomously perform their tasks with closed-loop controls.

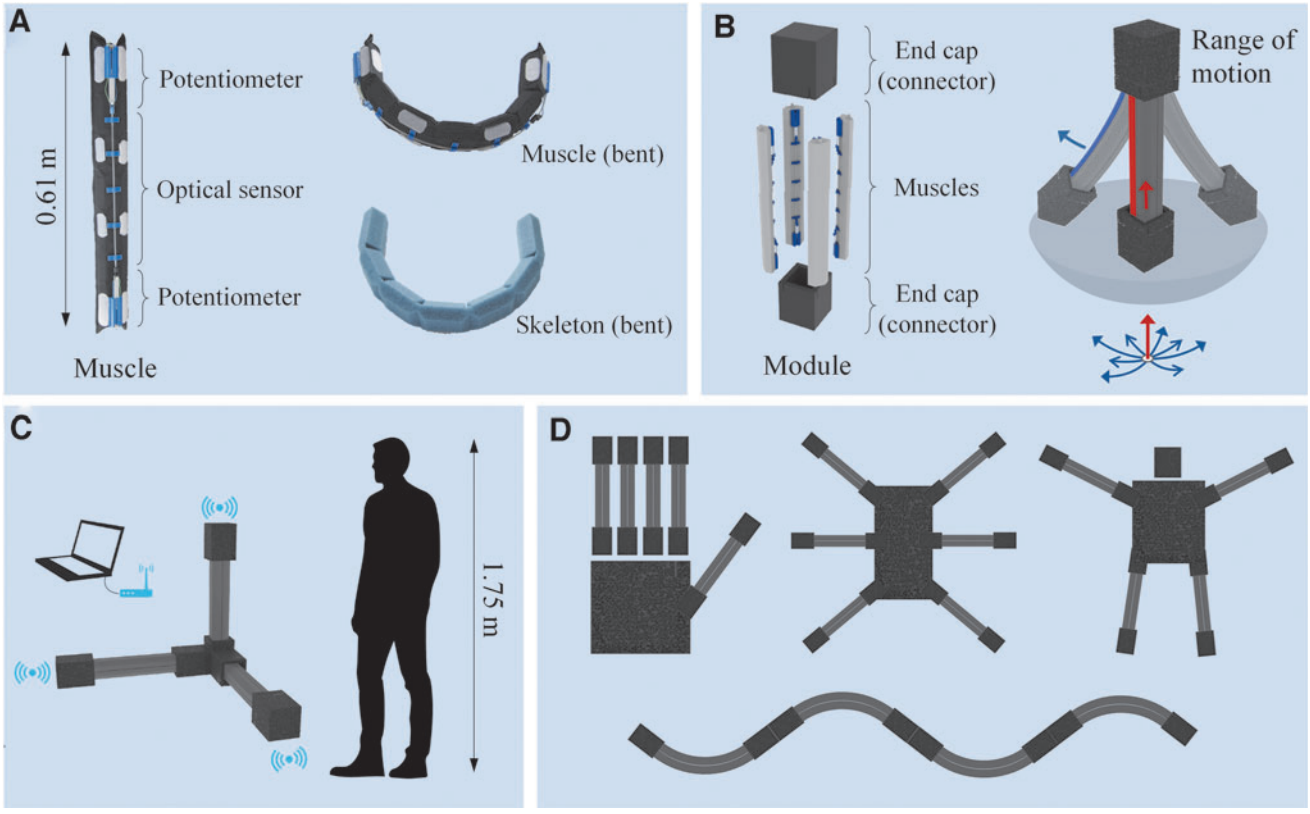

FIG. 1. Modular platform for large-scale untethered soft robots. **(A)** A single muscle (unactuated and actuated). Optical sensor and potentiometers are highlighted. Since this mechanism can produce forces only in one direction, four are combined in a module, as shown by the exploded view in **(B)**. This arrangement allows bending motion in eight directions, as well as contraction, as depicted in the same panel. Several of these modules can be combined together to build meter-scale soft robots. One example is shown in **(C)**. This tripod-like robot consists of three soft modules, and these modules can talk to each other and to an external base station through wireless connections. **(D)** A collection of other large robot designs that can be built using the proposed framework.

Results

A primary goal in designing this soft module was to achieve sufficiently high actuation strength and low weight to enable a single module to manipulate itself and several neighboring modules. To achieve this goal, we propose a solution based on fluid-driven origami-inspired artificial muscles (FOAMs) introduced in our previous study.[37] This class of soft actuators can produce high forces by utilizing vacuum pressure, and similar vacuum-based actuators have been discussed in other studies recently.[32,38–40] Most importantly, we have demonstrated that FOAM-based actuators are feasible for building multiscale robots that can be both soft and strong.[37,41,42] The proposed manufacturing method allows us to quickly fabricate and implement FOAM-based actuation systems at large scales. Therefore, this technology provides a very promising solution for scaling up soft robots.

In our design, each module functions as an independent unit made up of four ''muscle'' segments (FOAM-based soft actuators) for bending and a mechanism for linking to other modules. A typical FOAM actuator consists of an airtight thin membrane (the ''skin'') encasing a collapsible internal structure (the ''skeleton''). For each actuator in the module, its skin is made of inextensible nylon fabric sheets (heat-sealable nylon taffeta, thickness ≈ 0.24 mm), providing resistance to tearing, and the ability to withstand high tensile loads, while remaining compliant and lightweight. The skeleton is made of low-density polyethylene foam (density $\approx 28.8\,\mathrm{kg/m^3}$), to resolve trade-offs between compliance and strength, and high resilience and density. To allow for bidirectional flexion, we shape the skeleton backbone as a hexagonal prism, with strategically placed isosceles trapezoidal prism gaps and triangular prism divots (Figs. 1A and 8). Similarly to the skeleton of animals, this structural element also guides motion. When air is removed from the skin encasement, the sides of the cutouts bend toward each other while the back with no cutouts is effectively constrained as it has limited compression capabilities. As a result, the structure bends toward the gaps. However, each artificial muscle actuator can only bend and produce force in one direction (Supplementary Movie S1). We overcome this limitation by arranging four actuators into a single module so that each actuator bends outward, away from the central axis of the module (Fig. 1B).

In addition to the four muscle segments, each module contains its own vacuum pump, wireless communication system, low-level control system, and power source (rechargeable battery). Two cubic caps serve as connecting elements on both ends of the module, and they also house all of the pneumatics and electronics (Figs. 9 and 10 in Materials and Methods section). These end caps are made of the same polyethylene foam used for the skeleton. Velcro around the exterior of the end caps allows the module to attach to other modules in any configuration. The total weight of a single module is 1.6 kg. The length of each muscle is 0.6 m, and the full module is 0.86 m long. The cross section of each module is $0.15\,\mathrm{m} \times 0.15\,\mathrm{m}$. All material and components are selected to be low cost and easy to fabricate.

To control the bending of the module, a pneumatic circuit made up of a network of four solenoid valves is constructed that individually actuates each muscle (Fig. 10 in Materials and Methods section). Each of the actuators opens to the vacuum pump when its valve is switched on, and to atmospheric pressure when the valve is closed. These valves can be switched on and off at a high frequency by the microcontroller, allowing for pulse-width modulation (PWM) to create intermediate pressures. The minimum negative pressure that can be produced on board is approximately −70 kPa.

When one of the four muscles in the module is activated, the remaining three are passively guided by it, and the module bends in the direction prescribed by the active element. If two adjoining muscles are activated at the same time, the module bends toward the middle of the two segments. The module bends with constant curvatures if there is no external load. The maximum bending angle of the module is 22° when only one segment is activated, and it becomes $\sim 30°$ when two adjacent segments are activated simultaneously (Supplementary Fig. S3 in Materials and Methods section). When the four muscles are actuated at the same time, the bending forces are canceled so the module only exhibits linear contraction and no bending (see the module's different motions in Supplementary Movie S2). This axial contraction can be up to 0.06 m, $\sim 7\%$ of its initial length. These patterns of activation are combined in a coherent framework by the control algorithm discussed hereunder.

We assessed the bending force by constraining the module's bending motion, and then measuring the maximum blocked force through a load cell at the module's tip. We considered two types of activation—all single actuators were tested independently, then each adjacent pair of actuators. The average forces measured are 17.8 ± 1.4 N for a single actuator, and 21.5 ± 2.0 N with two actuators, at the maximum onboard vacuum pressure (−70 kPa). We assessed the contractile force by constraining the linear contraction, and measuring the force using an Instron machine when all four actuators were on. The average contractile force is 194 ± 10 N for a single module at the maximum onboard vacuum pressure (Supplementary Figs. S1 and S2 in Materials and Methods section).

The sensor system in each soft module is made up of eight sliding potentiometers and four fiber optic sensors, placed along the four muscles. This sensor system can detect the soft module's bending motions in eight directions, as well as its longitudinal contraction (the details are shown in Fig. 8C in Materials and Methods section). The fiber optic sensors provide information on the bending direction. An LED and a phototransistor are attached to either end of an optical fiber that is roughened on one side (the top surface) by a laser cutter. As the fiber bends toward the roughened side, less light escapes, while more light escapes when the fiber bends away. This change in light intensity is measured by the phototransistor. The ends of the optical fiber are each connected to the slider of a potentiometer, which, in turn, are fixed to the ends of the muscle. The changing potentiometer resistance gives us information on the muscle's contraction.

We use here Δ_x, Δ_y, and δL parametrization for describing the soft robot's configuration.[43] These values map broadly to movements in the plane of the first and third actuator, of the second and fourth actuators, and of the overall elongation, respectively (Supplementary Fig. S4 and more details are in Materials and Methods section). These values are obtained from potentiometer measurements. The fiber optic sensors are used to implement a check of consistency. The maximum activation among the four sensors is taken as the direction of

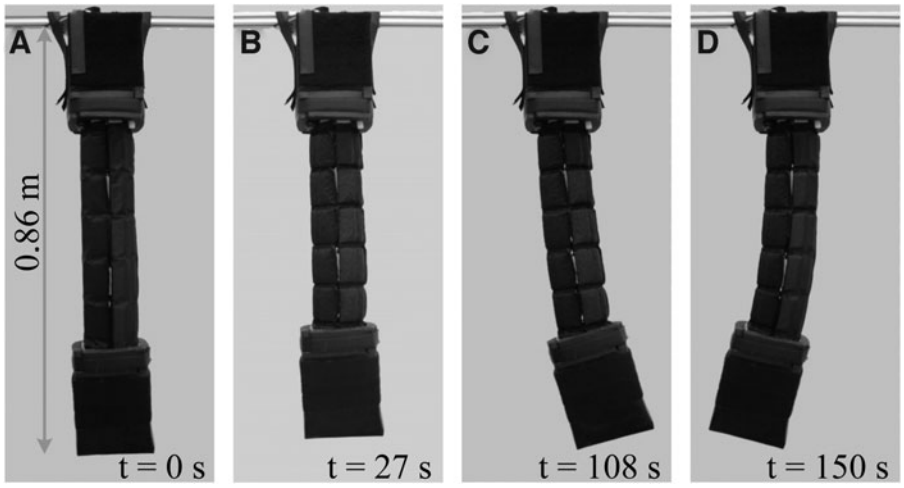

FIG. 2. Closed-loop control for a soft module. The robot starts at rest, as shown in **(A)**. Three reference configurations are then sequentially commanded to the robot. The resulting steady state configurations are shown in the same panel. The first is a pure contraction **(B)**, the second is a coordinated bending and contraction **(C)**, whereas the third is a pure bending with unconstrained contraction **(D)**.

bending, and compared with the values of Δ_x and Δ_y. Based on these sensor measurements, we implemented a feedback control strategy into each module. The controller is a proportional regulator with a leaky integrator and antiwind-up mechanism. The control action in the configuration space is first mapped to desired forces to be produced by the four muscles, and then transformed into duty cycles through an opportunely tuned sigmoidal function (more details are given in Materials and Methods section). To extend the range of reachable configurations, we consider two modes of operation: controlling all of the configurations (Δ_x, Δ_y, and δL), or controlling only the direction of bending. All configurations within the actuation constraints can be reached with steady state precision higher than 1%. Figure 2 shows a closed-loop control test on a soft module, and the sensor readings and experimental results are shown in Figure 3.

We demonstrate several untethered platforms built using the proposed technology. We investigate the use of the modules as legs, by creating a meter-scale walking creature that is made up of six modules attached to a foam sheet that makes up a body. The total body size of this robot is comparable with a large dog (with length, width, and height

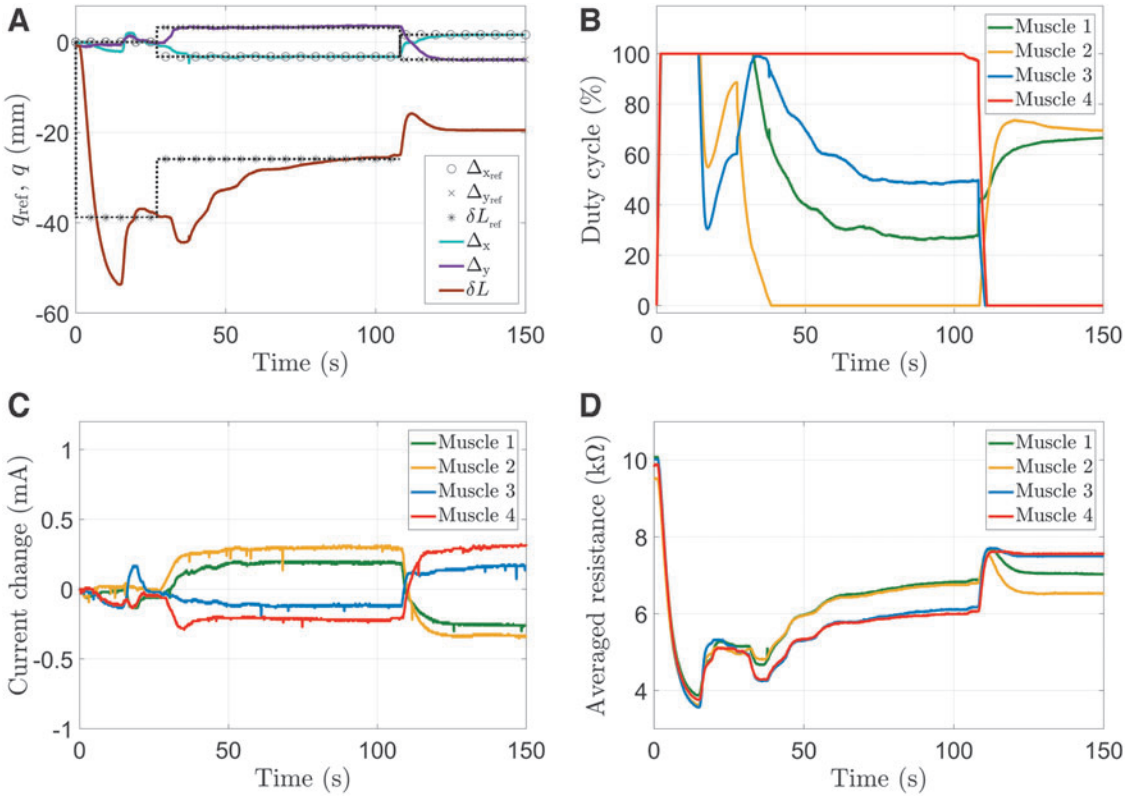

FIG. 3. Sensor readings and actuation during the closed-loop regulation. The observed posture of the robot is shown in **(A)** together with the reference values. The control actions (duty cycles) commanded to the four valves (muscles) are shown in **(B)**. **(C, D)** show the readings from the onboard optical fibers (change in electric current) and potentiometers (averaged resistance of two potentiometers on each muscle), during the closed-loop control test.

equal to 0.74, 0.43, and 0.92 m, respectively), as shown in Figure 4A and B. Standard gaits developed for rigid hexapods cannot be used to implement locomotion in this large soft robot.[44] These gaits assume rigid legs and, consequently, without considering the effects that we observed on real systems, such as buckling of the legs and uncontrolled tilting of the whole body. As an alternative to this approach, we devise a locomotion pattern inspired by the octopus.[45,46] Despite its symmetry, this animal uses preferentially two of its eight tentacles for legged locomotion on the ocean floor. We implement a similar pattern by using only the two front legs to advance. However, all the legs have a fundamental role in maintaining the robot's stability. Thus, in the gait we devised, only one leg is off the ground at any given time. Furthermore, all legs push the robot's body forward during the last phases of locomotion (Fig. 5 and Supplementary Movie S3). We tested this system on several surfaces—stone, grass, sand, and wood—to showcase the adaptability provided by the inherent compliance of the modules (Fig. 4C and Supplementary Movie S4).

Soft robotics is growing in importance for object grasping.[47–49] Soft hands can adapt to the object to be grasped, without the need of complex perception systems and control algorithms. Here we propose a large-scale soft gripper (1.7 m long) made of three modules, two of which are used as fingers. The robot is able to grasp and hold several large size objects with different shapes (Fig. 6 and Supplementary Movie S5). We also investigated other kinds of miscellaneous motions as shown in Figure 7 and Supplementary Movies S6–S8. To demonstrate a different type of locomotion, we built a four-limbed crawling robot. Two pairs of the soft modules are attached end to end so that the four end caps form a rectangular ''body'' in the middle with a pair of legs sticking out on either side. For this configuration, a crawling motion is achieved when all modules perform synchronized circular motions (locomotion speed $\approx$19 cm/min; see Fig. 7A–C and Supplementary Movie S6). Finally, we built a robotic rocking chair, made up of four soft modules as legs, and two sheets of foam as seat and backing. The chair is capable of lowering and raising itself and rocking, as a result of the coordinated motions of the legs (Fig. 7D–F and Supplementary Movie S7).

Discussion

Although we demonstrated several robotic configurations for possible applications, the proposed modules still present limits in terms of speed and durability. For the FOAM-based soft robots, the larger the actuator, the more air needs to be removed from the actuator to achieve sufficient bending and contractile motions. To maintain the actuation speed, pumps and valves with higher flow rates are required, including the associated larger size tubing and connectors, when the soft actuator is scaled up.

However, the size, weight, and power source of the onboard pneumatic system are constrained by the soft module's overall design. Therefore, we integrated a miniature onboard pneumatic system into each soft module, which includes a

FIG. 4. Meter-scale untethered hexapod robot. **(A, B)** A large-scale legged soft robot, built using six soft modules as the legs and a sheet of foam as the body. We investigated the locomotion strategy for this large soft robot on several different types of surface, such as grass, sand, and stone, as shown in **(C)**.

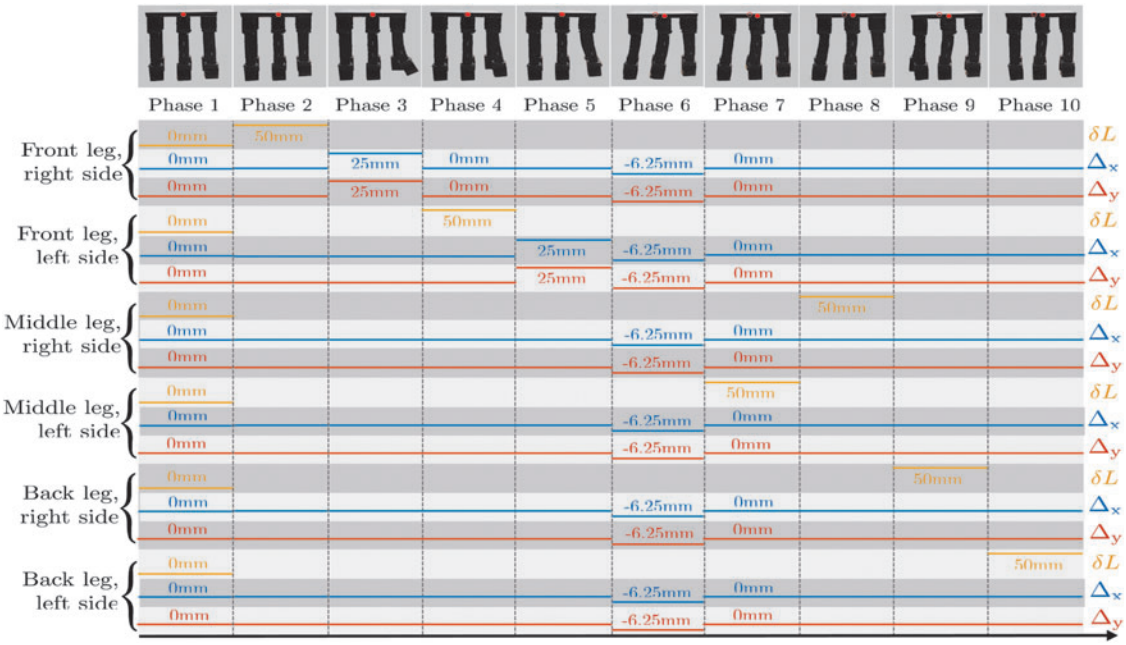

FIG. 5. Locomotion strategy and control for the large hexapod robot. Inspired by the locomotion of the octopus, the robot starts from a relaxed configuration (phase 1). The two front legs are then moved forward through a sequence of contraction, bending forward, and relaxing (phases 2 and 3 for the right leg, and phases 4 and 5 for the left). Subsequently, all six legs bend backward, pushing the robot's body forward (phase 6). Finally, the four back legs are sequentially contracted and relaxed so to put them in place (phases 7, 8, 9, and 10). The cycle then starts back from the beginning. *Red dots* indicate the evolution of the top sheet's center during locomotion (locomotion speed ≈ 4.5 cm/min, gait cycle ≈ 200 s).

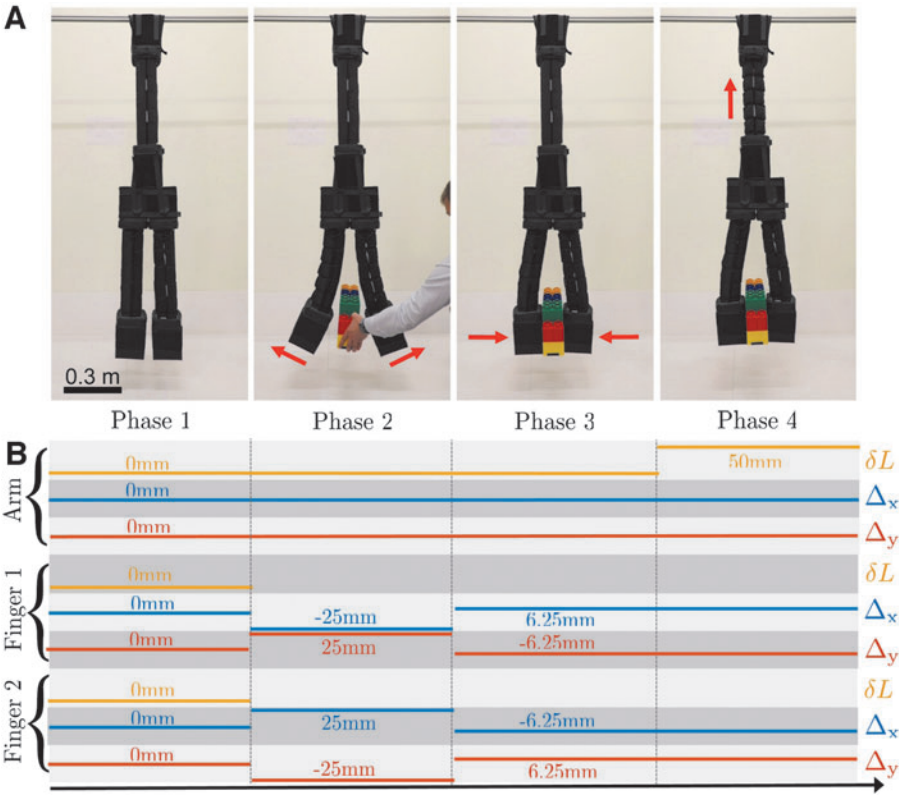

FIG. 6. Large-scale two-finger gripper. **(A)** The motion sequence (resting, opening, gripping, and lifting) of a large-scale two-finger gripper built using three of our soft modules. The corresponding control signals are shown in **(B)**.

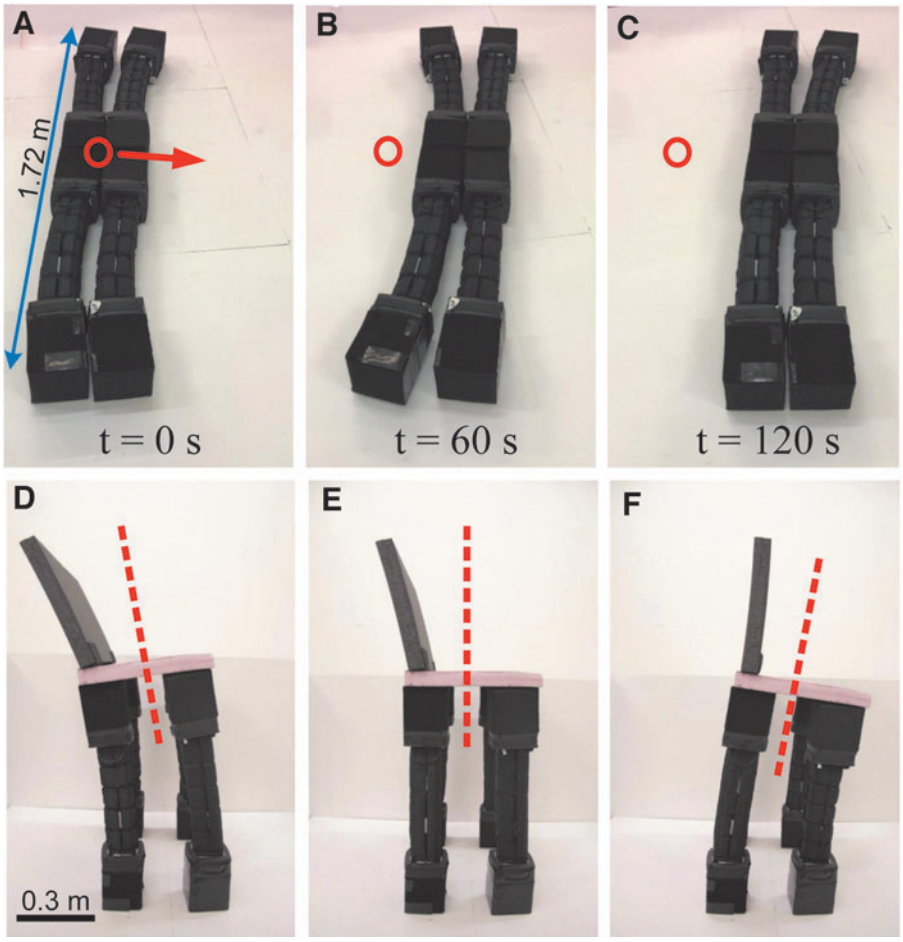

FIG. 7. Collection of other large-scale platforms. **(A–C)** A crawling robot made of four soft modules. The *red circle* indicates the starting location of the robot. **(D–F)** show a robotic chair, which by coordinated activation of its active legs can tilt backward and forward. The *dashed line* indicates the normal in the center of the seat.

vacuum pump and four solenoid valves connected by flexible and thin tubing. Owing to those design factors and hardware configuration, the actuation speed of the current soft module is relatively low, and it consequently causes slowness in our large robot applications, such as the hexapod locomotion. To increase the actuation speed of our soft module, we plan to implement a better performing pneumatic system (including pump, valves, and tubing) with lighter weight and higher flow rate. Furthermore, the muscle's skeleton structure could also be optimized for quicker and more efficient actuation, for example, using fewer or smaller structural voids to achieve the desired bending motion.

Also, we noticed a reduction in the performance of each module after prolonged use. This issue can be solved by leaving the robot at rest for few hours. This effect is likely due to the hysteretic nature of the foam materials we used. During each contraction, the foam expels air from its pores and is not able to immediately reacquire it when relaxed for short durations. We believe that this issue can be addressed by using better materials for the skeleton (e.g., more durable foam) and skin (e.g., thinner fabric sheet).

Conclusion

In this study, we developed large-scale vacuum-driven soft robotic modules that can bend in multiple directions, contract longitudinally, and connect to other modules. Each soft module is equipped with onboard actuation, proprioceptive sensing, intermodule communication, and computation. We demonstrated that these modules can be reconfigured into different human-scale soft robots on demand, such as a hexapod robot, a large gripper, and a crawling robot. Moreover, we developed closed-loop control algorithms that enable these meter-scale soft robots to autonomously perform their tasks. In the future, these large soft robots can be used for search and rescue, medical assistance, entertainment applications, etc.

Despite the aforementioned limitations, the experimental results in this article clearly show that soft robotic technology can extend its realm of application from small to large scales. This shift represents an important step toward moving soft robotics from the laboratory to environments designed for humans, a necessary leap for creating safer robot–human interactions and fulfilling the fundamental goal and promise of soft robotics.

Materials and Methods

Fabrication of the soft module

In our design, a complete soft module consists of four bending actuators and two end caps. The single bending actuator (''muscle'') is a foam ''skeleton'' wrapped in nylon fabric ''skin'' with a custom bending and contraction sensor system attached. The ideal materials for the skeleton have to meet the requirements for compliance, sufficient strength, high resilience, and lightweight. Similarly, the ideal skin

Table 1. Primary Materials Used in the Soft Modules

Component	*Material choice*	*Material properties*
Skin	TPU-coated nylon taffeta sheet	Thickness: 0.24 mm Density: 170 g/m^2 Others: heat sealable and airtight
Skeleton	Polyethylene foam sheet	Thickness: 5.08 cm Density: 28.8 kg/m^3 Tensile strength: 207 kPa Pressure to compress 25%: 48 kPa Others: closed-cell construction
End cap	Polyethylene foam sheet	Thickness: 1.27 cm Density: 35.2 kg/m^3 Tensile strength: 207 kPa Pressure to compress 25%: 62 kPa Others: closed-cell construction

TPU, thermoplastic polyurethane.

materials need to be flexible, airtight, nonstretchable, and lightweight; moreover, the skin materials should also provide resistance to tearing, and the ability to withstand high-tensile loads. The primary materials we used in this system are listed in Table 1. These specific materials were carefully chosen to create a simple, inexpensive, and easy-to-fabricate system.

Soft polyethylene foam sheets were used to fabricate the skeletons, and each foam sheet has an original dimension of 60.96 cm × 60.96 cm × 5.08 cm. To maximize the muscle's dimension, the foam sheet was first cut into 5.08 cm × 5.08 cm × 60.96 cm square prisms, which were then placed into a laser-cut mask. This acrylic-based mask is a guide for hot-wire cutting the foam structure with the designed geometric pattern. All parts not covered by the mask were then cut off from the beam, and the finished skeleton structure is shown in Figure 8A.

The back edge of the beam is cut to make a flat surface to facilitate the embedded electronics as well as to reduce the actuator stiffness. Triangular divots were cut opposite to the rectangular gaps in the front surface (Fig. 8B). These divots allow for flexion in the backward bending direction of each muscle. This is a necessary setup to allow for the eight directions of bending on a full module with four bonded muscles. To enhance air flow through the skeleton, holes were drilled through the solid blocks in the end of skeleton along its spine. A nylon nut was then glued inside one of the edge blocks for connection to the exterior of the actuator.

The estimated critical load for each soft module is >45 N, based on the skeleton materials' properties listed in Table 1. This result indicates that each module can vertically withstand the weight of at least another three soft modules (total height >3.4 m) without buckling.

A thin nylon fabric sheet, with thermoplastic polyurethane coating on one side, was then heat sealed to tightly enclose the skeleton. A single hole was later cut in the skin to connect a threaded tube coupler to the interior nut, with a flexible rubber washer intermediate to ensure an airtight connection. A set of short Velcro strips were attached onto the top surface of the bending actuator to provide easy, reliable, and flexible coupling between the muscles.

On the backside of the actuator, the sensors are held on through a set of 3D-printed parts, including two parts to hold sliding potentiometers on both ends, and five guides with holes to constrain the optical fiber along the actuator. A transparent plastic tube of 0.3 cm diameter was glued to the printed guides, and then the optical fiber was threaded through it. The fiber sensor was then connected to the sliding parts of the potentiometers at both ends. This tube allows

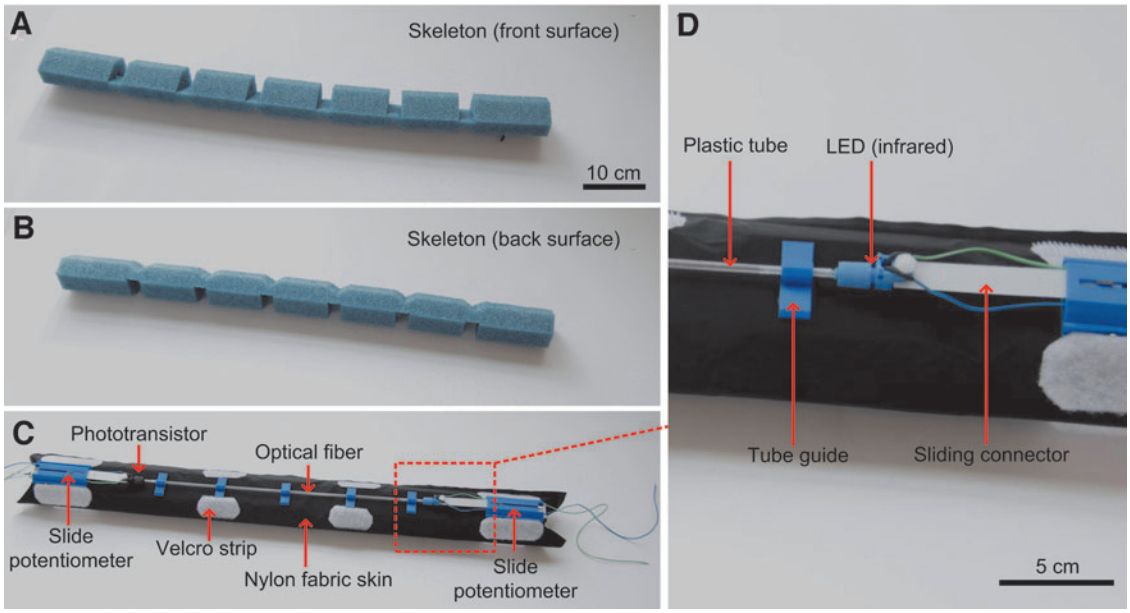

FIG. 8. Single muscle fabrication. The front **(A)** and back **(B)** surfaces of a foam-based skeleton cut by a hot-wire cutter. **(C)** A complete bending actuator with bending sensors.

the optical fiber to freely float between the sliding potentiometers, while it also constrains the fiber to the middle of the actuator (Fig. 8C, D).

The end caps enclose the battery, microcontroller board, pump, and valves. In addition, these box-shaped caps allow for structural connections between the soft modules. Each of the end caps is made of five 1.27-cm-thick foam pieces as shown in Figure 9A. These foam pieces were cut with rectangular notches to allow for an easy and secure assembly (Fig. 9B). The outer surface of the assembled cap was wrapped in duct tape to further hold the foam pieces together. We then covered the outer surface with nylon fabric-based Velcro sheets (adhesive backed), alternating hooks, and loops for each side (Fig. 9C). It should be noted that we left a 5-cm-wide area without wrapping on the top of each side wall. This design provides some extra space for inserting and removing the muscle bundle. Velcro strips were then attached to the inside surface of these side walls, thus the cap can be securely attached onto the muscle bundle (Fig. 9D).

Pneumatics and electronics

Unlike most pneumatic-driven soft robots that must be tethered to a pneumatic power source (usually compressed air for positive pressure), our module is capable of carrying an onboard pump. A miniature vacuum pump (voltage: 12 V DC, maximum flow rate: 15 LPM) supplies the negative pressure input to all of the actuators, and the flow is divided among all of the activated actuators. To control the bending of the module, a pneumatic circuit made up of a network of four solenoid valves was constructed that allows for the individual actuation of each muscle in a module (Fig. 10). Actuators are each connected to a three-way two-position valve that opens to the pump when the valve is on, and vents to atmospheric pressure when off. These valves can be turned on and off at a high frequency (up to 50 Hz) by the microcontroller, allowing for PWM to create intermediate pressures.

The electrical system is responsible for powering all the onboard components and provides the brain for control and communication. It consists of a Li-ion rechargeable battery (7.4 V, 2600 mAh), a microcontroller (Arduino Mega 2560), a wireless communication module (XBee S1), a single-MOSFET pump driver, a 4-valve driver circuit, a 12-channel sensor readout circuit, and a power switch. The Arduino board can be powered by the raw battery voltage, and a step-up regulator is used to boost the supply voltage to 12 V for the vacuum pump and valves (Fig. 10).

The Arduino microcontroller is responsible for switching the pumps and valves on and off and can dictate the motion of the system. Turning on a valve opens the corresponding pneumatic actuator to the vacuum pump, which causes the actuator to bend. By assigning which valves are on at any given time, the Arduino can control the direction of bending of the module. In addition, as mentioned before, the valves are capable of PWM so the Arduino can also control intermediate degrees of bending for each actuator.

Finally, the Arduino is connected to an XBee communication device that allows all modules to send and receive data (or commands) wirelessly. This setup can be used to implement wireless control, whereby a user can send actuation inputs to the modules and dictate desired motions manually. Alternatively, communication signals between the modules can be used to autonomously synchronize or coordinate the motions of the modules.

The set of sensors for each actuator included two sliding potentiometers (10 kΩ, linear taper), placed on the ends of the actuator, with a fiber optic bending sensor connecting the two together. To build an optical bending sensor, we roughened one side (the top surface) of an unjacketed 2-mm-diameter optical fiber using the raster setting on a laser cutter.[50–52] An IR LED (IF-E91A; Industrial Fiberoptics, Inc.) was then attached to one end of the fiber, and a phototransistor (IF-D92; Industrial Fiberoptics, Inc.) was connected to the other end, along with a sensor readout circuit (voltage divider) for the Arduino. A thin flexible plastic strip was used to connect the slider of the potentiometer to the base of the LED or phototransistor. This setup ensures these pieces move in tandem, causing the sliding potentiometers to move out and decrease in resistance when the single actuator bends or contracts (Figs. 8C, D and 10B).

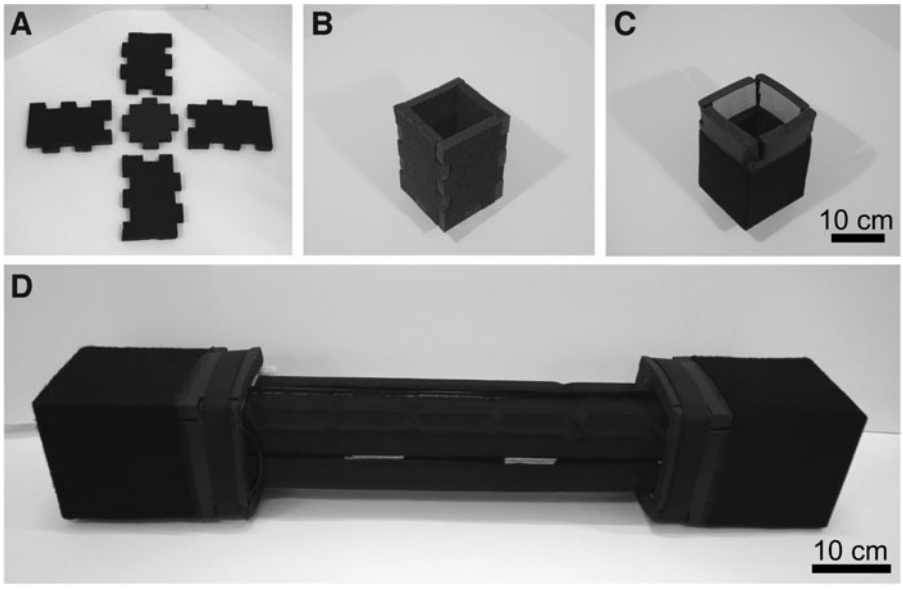

FIG. 9. Assembly process of the module end cap. **(A)** Interlocking pieces of foam are cut by a hot-wire cutter, **(B)** putting the pieces together and **(C)** wrapping the end cap with duct tape and adhesive-backed Velcro. **(D)** A fully assembled soft module with four muscles and two end caps.

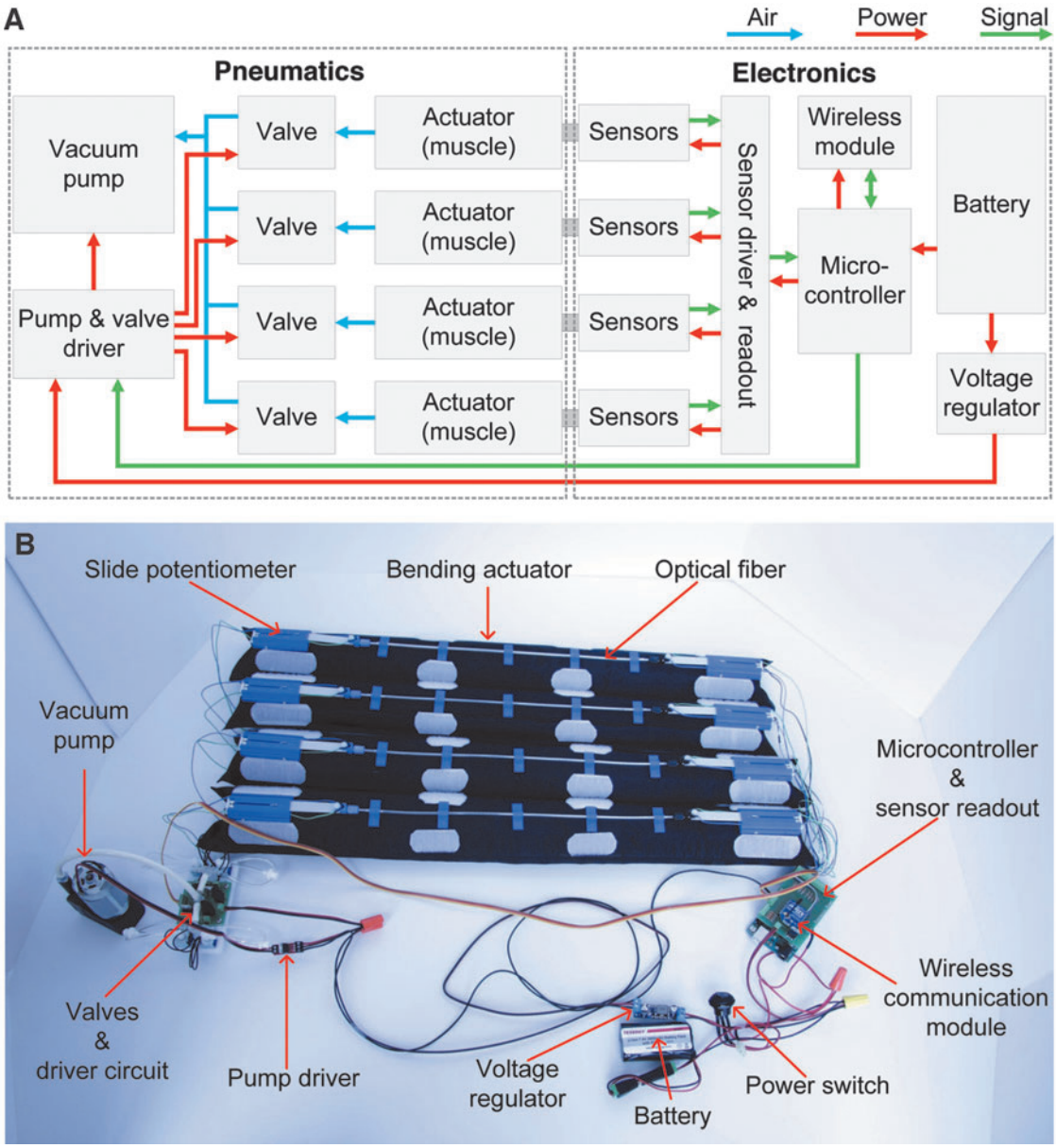

FIG. 10. The pneumatics and electronics of the soft module. **(A)** A block diagram of our soft module system. **(B)** The key components in a soft module.

Force and bending characterizations

The soft module consists of four bending muscles, and each muscle can only bend toward one diagonal direction (or lateral edge) of the module (Fig. 1 and Supplementary Fig. S4). Owing to this arrangement, each soft module can only produce a set of useful motions using particular combinations of the four muscles, including the single-muscle bending, dual-muscle bending, and four-muscle contractile motions. It should be noted that the soft module cannot produce contraction using a single muscle or a pair of muscles.

We performed two types of blocked force test under different actuation modes. The first was a bending force test, in which we constrained the module so that it could not bend upon actuation, and measured the maximum force exerted at the tip of the module using a load cell (FC2231-0000-0010-L). In this test, the particular combinations of a subset of actuators turned on in the module at a time. For example, all four actuators were tested independently (single-muscle test), then each adjacent pair of actuators was tested (dual-muscle test). Supplementary Figure S1A and B shows the averaged results based on four measurements on a soft module using these two kinds of combinations.

The second was a contractile force test in which we constrained linear contraction and then measured the axial contractile force of a soft module using an Instron universal testing machine (Instron 5944; see Supplementary Fig. S2A). In this case, each of the four actuators was switched on, and their bending forces canceled out so the module only exhibited linear contraction without bending. Three soft modules were used in our measurements, and the averaged results are shown in Supplementary Figure S1C.

Owing to the diagonal arrangement of the four muscles in each module, the muscles' bending forces will be partially canceled if they are activated at the same time. Therefore, the force produced by the dual-muscle bending is not two times the force produced by the single-muscle bending. Instead, the resulting force is a combination of the bending forces produced by the two muscles in two different directions. We believe that the hysteresis phenomena of the soft module are most likely due to the compression of the foam-based skeleton structures, as well as the friction between the skeleton and skin materials.

During the tests, the end caps were attached with Velcro to either the Instron or the custom built blocking setup made from aluminum beams (Supplementary Fig. S2B). These setups are designed to constrain any motion in the direction of the measured load. The applied pressures were measured by a digital vacuum pressure sensor (MPXV6115VC6U-ND). Each measurement was a full cycle from pressure equilibrium between inside and outside of the actuator to the maximum vacuum pressure of −70 kPa and then back to the equilibrium pressure (0 kPa).

To analyze the relationship between the applied vacuum pressure and bending angle of the module, a soft module was suspended upside down in a motion capture room as shown in Supplementary Figure S3A. We applied pressure in steps of −10 kPa going from 0 to −70 kPa for both single and double actuator bending modes, setting and maintaining the pressure with a pressure regulator. At each pressure level, all the actuators were activated one by one, with periods of rest in between. For the single-muscle bending, each actuator was activated for 10 s with 10 s of rest, whereas for the dual-muscle bending, each pair of two actuators was activated simultaneously with 20 s of actuation and 20 s of resting. The time was adjusted so that the module could reach its maximum bending angle during activation as well as relax back to no bending while resting. The rotation and position of the bottom cap of a soft module were tracked by a Vicon motion tracking system. The angle of bending is defined as the angle θ between the normals of the top and bottom surfaces of the module in its bending plane (Supplementary Fig. S3A). Supplementary Figure S3B shows the averaged experimental results over four trials of tests for each bending mode.

Controller design

The controller is developed based on the Piecewise Constant Curvature hypothesis, under which the robot can be approximated as an interconnection of modules with constant curvature in space, but variable in time.[53] In this study, we assume that each soft module bends with constant curvature in a robot configuration. We should note that three effects may spoil the constant curvature assumption, including dynamic motion, nonconstant stiffness along the segment, and gravity. The system moves slowly enough to neglect dynamic forces that would generate a nonconstant strain. Also, the foam skeleton's flexural stiffness is reasonably homogeneous along the segment. Finally, the foam-based structure is relatively light weight, so gravity does not generate the discussed effect.

To describe the robot configuration, we use here the parametrization proposed in our previous work,[43] which uses three variables per module (Supplementary Fig. S4). The first variable is $\Delta_{x,i} \in \mathbb{R}$, which measures the bending in the plane of the first and third actuator as the difference between two constant curvature arches virtually connected to the two actuators. $\Delta_{y,i} \in \mathbb{R}$ is similarly defined with the second and fourth actuator. $\delta L_i \in \mathbb{R}$ is the overall elongation of the module with respect to the rest condition. We call the vector containing these values for all modules $q \in \mathbb{R}^{3n}$, the configuration of the entire robot, made of n modules.

The control strategy is built as an interconnection of three subalgorithms, as shown by Supplementary Figure S5; output mapping, controller, and input mapping. At each control iteration, all three algorithms are executed. The first algorithm is the output mapping, which estimates the robot configuration q from the four elongation sensors, for each module:

$$\begin{aligned} L &= 2I_{\mathrm{o}}(y) + L_0, \\ \Delta_{x,i} &= \frac{L_i[3] - L_i[1]}{2}, \\ \Delta_{y,i} &= \frac{L_i[2] - L_i[4]}{2}, \\ \delta L_i &= \frac{\sum_{j=1}^{4} L_i[j]}{4} - L_{0,i}, \end{aligned} \tag{1}$$

where $L_i[j]$ is the length of the j-th arc—where the j-th sensor is placed—of the i-th module. L is the vector containing all the $L_i[j]$. $L_{0,i}$ is the same module's length at rest. $I_{\mathrm{o}} : \mathbb{R}^{4n} \to \mathbb{R}^{4n}$ is a function inverting the physical characteristics of the resistance sensors. We consider it here to be an affine transformation. A more complex nonlinear black box model could be used as well (e.g., artificial neural networks). The offsets and the slopes in I_{o} are evaluated through a pseudoinverse of the regressor matrix built using data collected from direct sensor outputs, and the actual robot pose as determined by a Vicon motion tracking system. In these experiments, every subset of adjacent actuators is actuated at different PWM levels (25%, 50%, 75%, and 100%) to capture a range of directions and degrees of bending. As a test of consistency, we evaluate, at each time step, the curvature resulting from the estimated configuration:

$$\theta_i = \frac{\sqrt{\Delta_{x,i}^2 + \Delta_{y,i}^2}}{\Delta_{s,i}}, \tag{2}$$

where $\Delta_{s,i}$ is the distance between the elongation sensors and central axis of the module, measured on the cross section (Supplementary Fig. S4). We then compare it with the direct readings coming from the four curvature sensors. If the difference between the two is consistently higher than 25% for >1 second, then an error exception is thrown.

The second subalgorithm is the core controller. We use here a leaky proportional–integral–derivative (PID) regulator, where the leaky part is instrumental to deal with saturation of the actuators and unmodeled interactions with the environment. The following equations describe this controller:

$$\begin{aligned} \dot{\varepsilon} &= q_{\mathrm{ref}} - q - L\varepsilon, \\ u &= P(q_{\mathrm{ref}} - q) + I\varepsilon - D\dot{q}. \end{aligned} \tag{3}$$

The first equation implements the leaky integration, with $\varepsilon \in \mathbb{R}^{3n}$. $L \in \mathbb{R}^{3n \times 3n}$ is a diagonal matrix, serving as leaking constant, which can be changed dynamically depending on the task currently executed by the robot. $u \in \mathbb{R}^{3n}$ is the control action in the q-space, and q_{ref} is the desired robot

configuration. We subtract from the integrator $-M_{\mathrm{D}}^{\mathrm{T}}w$, where $w = u$ if $u < 0$, and 0 otherwise (antiwind-up mechanism). Note that q_{ref} can be either directly specified or evaluated using standard kinematic inversion algorithms. $P, I, D \in \mathbb{R}^{3n\times 3n}$ are diagonal gain matrices.

Finally, the control action u in Equation (3) is transformed into commands for the actuators, as $d(t) = S(M_{\mathrm{inv}}u(t))$. The matrix $M_{\mathrm{inv}} \in \mathbb{R}^{4n\times 3n}$ maps the actuation from q-space to the actuation space. It is a block diagonal matrix having as the i-th block:

$$M_{\mathrm{inv},i} = \begin{bmatrix} -\frac{1}{2\Delta_{a,i}} & 0 & \frac{1}{4} \\ 0 & \frac{1}{2\Delta_{a,i}} & \frac{1}{4} \\ \frac{1}{2\Delta_{a,i}} & 0 & \frac{1}{4} \\ 0 & -\frac{1}{2\Delta_{a,i}} & \frac{1}{4} \end{bmatrix}, \tag{4}$$

where $\Delta_{a,i}$ is the distance between the center of the muscles and the center of the module, measured on the cross section (Supplementary Fig. S4). The function $S : \mathbb{R}^{4n} \to \mathbb{R}^{4n}$ is used to go from forces to duty cycles. We do that by mapping all the elements of the input vector through the function $100(e^{4u_i} - 1)/(e^{4u_i} + 1)$ if $u_i > 0$, and 0 otherwise. The parameter of the sigmoid function was chosen by fitting the inputs and outputs of the actuators, using the least square method.

Acknowledgments

We thank Scott B. Mandelbaum, Logan S. Stafford, and Brooke C. McGoldrick at MIT for their help on the development of the robot prototypes. We also thank Daniel Vogt and Huichan Zhao at Harvard University for their help and suggestions on this study.

Disclaimer

Any opinions, findings, and conclusions or recommendations expressed in this material are those of the authors and do not necessarily reflect the views of the National Science Foundation.

Author Disclosure Statement

No competing financial interests exist.

Funding Information

This study was supported, in part, by the National Science Foundation (Grant Nos. 1830901 and 1226883) and Amazon Robotics.

Supplementary Material

Supplementary Figure S1
Supplementary Figure S2
Supplementary Figure S3
Supplementary Figure S4
Supplementary Figure S5
Supplementary Movie S1
Supplementary Movie S2
Supplementary Movie S3
Supplementary Movie S4
Supplementary Movie S5
Supplementary Movie S6
Supplementary Movie S7
Supplementary Movie S8

References

1. Rus D, Tolley MT. Design, fabrication and control of soft robots. Nature 2015;521:467.
2. Kim S, Laschi C, Trimmer B. Soft robotics: a bioinspired evolution in robotics. Trends Biotechnol 2013;31:287–294.
3. Iida F, Laschi C. Soft robotics: challenges and perspectives. Proc Comput Sci 2011;7:99–102.
4. Laschi C, Mazzolai B, Cianchetti M. Soft robotics: technologies and systems pushing the boundaries of robot abilities. Sci Robot 2016;1:eaah3690.
5. Ilievski F, Mazzeo AD, Shepherd RF, *et al.* Soft robotics for chemists. Angew Chem Int Ed 2011;50:1890–1895.
6. Miriyev A, Stack K, Lipson H. Soft material for soft actuators. Nat Commun 2017;8:596.
7. Nelson BJ, Kaliakatsos IK, Abbott JJ. Microrobots for minimally invasive medicine. Annu Rev Biomed Eng 2010; 12:55–85.
8. Hu W, Lum GZ, Mastrangeli M, Sitti M. Small-scale soft-bodied robot with multimodal locomotion. Nature 2018; 554:81.
9. Tolley MT, Shepherd RF, Mosadegh B, *et al.* A resilient, untethered soft robot. Soft Robot 2014;1:213–223.
10. Lin H-T, Leisk GG, Trimmer B. Goqbot: a caterpillar-inspired soft-bodied rolling robot. Bioinspir Biomim 2011; 6:026007.
11. Shepherd RF, Ilievski F, Choi W, *et al.* Multigait soft robot. Proc Natl Acad Sci 2011;108:20400–20403.
12. Cianchetti M, Ranzani T, Gerboni G, *et al.* Soft robotics technologies to address shortcomings in today's minimally invasive surgery: the stiff-flop approach. Soft Robot 2014; 1:122–131.
13. Bar-Cohen Y. Electroactive Polymer (EAP) Actuators as Artificial Muscles: Reality, Potential, and Challenges, Vol. 136. SPIE Press, Bellingham, Washington, USA, 2004.
14. Kim KJ, Tadokoro S. Electroactive polymers for robotic applications. Artif Musc Sens 2007;23:291.
15. Hawkes EW, Blumenschein LH, Greer JD, *et al.* A soft robot that navigates its environment through growth. Sci Robot 2017;2:eaan3028.
16. Usevitch NS, Hammond ZM, Schwager M, *et al.* An untethered isoperimetric soft robot. Sci Robot 2020;5: eaaz0492.
17. Takeichi M, Suzumori K, Endo G, *et al.* Development of giacometti arm with balloon body. IEEE Robot Autom Lett 2017;2:951–957.
18. Sanan S, Ornstein MH, Atkeson CG. Physical human interaction for an inflatable manipulator. In 2011 Annual International Conference of the IEEE Engineering in Medicine and Biology Society. Boston, USA: IEEE, 2011:401–7404.
19. Otherlab. https://www.otherlab.com (accessed December, 2019).
20. Best CM, Wilson JP, Killpack MD. Control of a pneumatically actuated, fully inflatable, fabric-based, humanoid robot. In 2015 IEEE-RAS 15th International Conference on Humanoid Robots (Humanoids). Seoul, South Korea: IEEE, 2015:1133–1140.
21. Hyatt P, Kraus D, Sherrod V, *et al.* Configuration estimation for accurate position control of large-scale soft robots. IEEE/ASME Trans Mechatron 2018;24:88–99.

22. Rich SI, Wood RJ, Majidi C. Untethered soft robotics. Nat Electr 2018;1:102.
23. Kier WM, Smith KK. Tongues, tentacles and trunks: the biomechanics of movement in muscular-hydrostats. Zool J Linnean Soc 1985;83:307–324.
24. Yim M, Shen W-M, Salemi B, *et al.* Modular self-reconfigurable robot systems [grand challenges of robotics]. IEEE Robot Autom Mag 2007;14:43–52.
25. Li S, Batra R, Brown D, *et al.* Particle robotics based on statistical mechanics of loosely coupled components. Nature 2019;567:361.
26. Vergara A, Lau Y-S, Mendoza-Garcia R-F, *et al.* Soft modular robotic cubes: toward replicating morphogenetic movements of the embryo. PLoS One 2017;12:e0169179.
27. Cheney N, MacCurdy R, Clune J, *et al.* Unshackling evolution: evolving soft robots with multiple materials and a powerful generative encoding. ACM SIGEVOlution 2014; 7:11–23.
28. Onal CD, Rus D. A modular approach to soft robots. In 2012 4th IEEE RAS & EMBS International Conference on Biomedical Robotics and Biomechatronics (BioRob). Rome, Italy: IEEE, 2012:1038–1045.
29. Kurumaya S, Phillips BT, Kaitlyn P, *et al.* A modular soft robotic wrist for underwater manipulation. Soft Robot 2018;5:399–409.
30. Kwok SW, Morin SA, Mosadegh B, *et al.* Magnetic assembly of soft robots with hard components. Adv Funct Mat 2014;24:2180–2187.
31. Germann J, Dommer M, Pericet-Camara R, *et al.* Active connection mechanism for soft modular robots. Adv Robot 2012;26:785–798.
32. Robertson MA, Paik J. New soft robots really suck: vacuum-powered systems empower diverse capabilities. Sci Robot 2017;2:eaan6357.
33. Fei Y, Gao H. Nonlinear dynamic modeling on multi-spherical modular soft robots. Nonlinear Dyn 2014;78:831–838.
34. Zou J, Lin Y, Ji C, *et al.* A reconfigurable omnidirectional soft robot based on caterpillar locomotion. Soft Robot 2018;5:164–174.
35. Zhang Y, Zheng T, Fan J, *et al.* Nonlinear modeling and docking tests of a soft modular robot. IEEE Access 2018;7: 11328–11337.
36. McKenzie RM, Sayed ME, Nemitz MP, *et al.* Linbots: soft modular robots utilizing voice coils. Soft Robot 2019;6: 195–205.
37. Li S, Vogt DM, Rus D, *et al.* Fluid-driven origami-inspired artificial muscles. Proc Natl Acad Sci 2017;114:13132–13137.
38. Yang D, Verma MS, So J-H, *et al.* Buckling pneumatic linear actuators inspired by muscle. Adv Mater Technol 2016;1:1600055.
39. Felt W, Robertson MA, Paik J. Modeling vacuum bellows soft pneumatic actuators with optimal mechanical performance. In 2018 IEEE International Conference on Soft Robotics (RoboSoft). Livorno, Italy: IEEE, 2018:534–540.
40. Tawk C, In Het Panhuis M, Spinks GM, *et al.* Bioinspired 3D printable soft vacuum actuators for locomotion robots, grippers and artificial muscles. Soft Robot 2018;5:685–694.
41. Li S, Stampfli JJ, Helen JX, *et al.* A vacuum-driven origami magic-ball soft gripper. In 2019 IEEE International Conference on Robotics and Automation (ICRA). Montreal, Canada: IEEE, 2019:7401–7408.
42. Li S, Vogt DM, Bartlett NW, *et al.* Tension pistons: amplifying piston force using fluid-induced tension in flexible materials. Adv Funct Mater 2019;29:1901419.
43. Della Santina C, Bicchi A, Rus D. On an improved state parametrization for soft robots with piecewise constant curvature and its use in model based control. IEEE Robot Autom Lett 2020;5:1001–1008.
44. Delcomyn F, Nelson ME. Architectures for a biomimetic hexapod robot. Robot Auton Syst 2000;30:5–15.
45. Huffard CL, Boneka F, Full RJ. Underwater bipedal locomotion by octopuses in disguise. Science 2005;307:1927–1927.
46. Calisti M, Giorelli M, Levy G, *et al.* An octopus-bioinspired solution to movement and manipulation for soft robots. Bioinspir Biomim 2011;6:036002.
47. Deimel R, Brock O. A novel type of compliant and underactuated robotic hand for dexterous grasping. Int J Robot Res 2016;35:161–185.
48. Shintake J, Cacucciolo V, Floreano D, *et al.* Soft robotic grippers. Adv Mater 2018;30:1707035.
49. Hughes J, Culha U, Giardina F, *et al.* Soft manipulators and grippers: a review. Front Robot AI 2016;3:69.
50. Zhao H, Huang R, Shepherd RF. Curvature control of soft orthotics via low cost solid-state optics. In 2016 IEEE International Conference on Robotics and Automation (ICRA). Stockholm, Sweden: IEEE, 2016:4008–4013.
51. Kuang KS, Cantwell WJ, Scully PJ. An evaluation of a novel plastic optical fibre sensor for axial strain and bend measurements. Meas Sci Technol 2002;13:1523.
52. Djordjevich A, Boskovic M. Curvature gauge. Sens Actuat A Phys 1995;51:193–198.
53. Webster III RJ, Jones BA. Design and kinematic modeling of constant curvature continuum robots: a review. Int J Robot Res 2010;29:1661–1683.

Address correspondence to:
Shuguang Li
John A. Paulson School of Engineering and Applied Sciences
Harvard University
Room 4.201
150 Western Avenue
Allston, MA 02134
USA

E-mail: lisg@seas.harvard.edu